AGU PUBLICATIONS

JGR

Journal of Geophysical Research: Atmospheres

RESEARCH ARTICLE

10.1002/2014JD022460

Influence of ENSO on the QBO: Results from an ensemble of idealized simulations

S. Schirber[1]

[1] Max Planck Institute for Meteorology, Hamburg, Germany

Key Points:
- ENSO modifies wave activity in the troposphere
- ENSO changes QBO amplitude
- ENSO changes QBO downward progression

Correspondence to:
S. Schirber,
sebastian.schirber@mpimet.mpg.de

Citation:
Schirber, S. (2015), Influence of ENSO on the QBO: Results from an ensemble of idealized simulations, *J. Geophys. Res. Atmos.*, *120*, 1109–1122, doi:10.1002/2014JD022460.

Received 18 AUG 2014
Accepted 13 JAN 2015
Accepted article online 19 JAN 2015
Published online 12 FEB 2015

Abstract The El Niño–Southern Oscillation (ENSO) changes convection in the tropics and therefore the excitation of equatorial waves. Equatorial waves propagate from the troposphere upward where they drive the quasi-biennial oscillation (QBO) in the stratosphere. In this work, we analyze the effect of ENSO on the QBO utilizing an atmospheric general circulation model in a comprehensive experimental setup. We construct two ensembles of different QBO initial conditions, with the onset of a westerly (QBOW) and easterly (QBOE) jet at 10 hPa. In the course of an 18 months simulation period, the two sets of initial conditions experience each El Niño (EL) and La Niña (LA) boundary conditions. Due to the increased tropospheric temperatures during EL conditions compared to LA conditions, the experiments show an increase in tropospheric wave activity which increases QBO forcing in the stratosphere in EL. The underlying easterly jet in QBOW is weaker during EL compared to LA, while the underlying westerly jet in QBOE is stronger during EL compared to LA. On one hand, the weaker underlying jet in QBOW and the increase in QBO forcing due to waves cause a faster downward propagation for the westerly jet in QBOW during EL. On the other hand, the stronger underlying jet in QBOE opposes the increased QBO forcing due to waves for QBOE during EL. Therefore, the downward propagation speed of the easterly jet in QBOE is similar during EL and LA conditions. Changes in stratospheric tropical upwelling associated with EL and LA do not affect QBO properties in the simulation.

1. Introduction

The quasi-biennial oscillation (QBO) of zonal winds is a prominent dynamical feature in the equatorial stratosphere [*Baldwin et al.*, 2001]. The QBO is driven by waves which emanate from tropospheric convection, propagate upward into the middle and upper atmosphere, and deposit momentum when breaking at the QBO shear zones below the jet maxima [*Lindzen and Holton*, 1968]. In the tropics, waves emanate from convection and variability in convection changes wave activity which in turn projects on the QBO [*Schirber et al.*, 2014a]. The tropical phenomenon El Niño–Southern Oscillation (ENSO) strongly changes the atmospheric and oceanic state on interannual time scales. The phenomenon originates in the Pacific and is characterized by two opposing phases of an oscillation, El Niño (EL) and La Niña (LA). In this work, we analyze how EL and LA events change tropospheric wave activity and how the anomalous wave forcing modulates the QBO in the stratosphere. The tool we choose to investigate the coupling of these two tropical phenomena on interannual time scales is the general circulation model (GCM) European Centre/Hamburg 6 (ECHAM6), which includes a physically based gravity wave (GW) parameterization.

In the tropics, anomalous sea surface temperatures (SSTs) lead to anomalies in precipitation [*Soden*, 2000]. Anomalous precipitation is a manifestation of changes in convective activity and consequently changes in the excited equatorial waves [*Bergman and Salby*, 1994; *Alexander and Holton*, 1997; *Tsuda et al.*, 2009]. In the case of ENSO, an increase in temperature and precipitation during EL is a manifestation of increased wave activity, and vice versa during LA [*Wang and Geller*, 2003; *Wang and Alexander*, 2010]. Anomalous tropospheric wave activity influences the two general QBO forcing mechanisms. On one hand, an increase in tropospheric wave activity during EL leads to an increase of stratospheric wave forcing of the QBO, and vice versa for LA [*Pfister et al.*, 1993]. On the other hand, an increase in wave activity during EL also leads to an intensification of the Brewer-Dobson circulation, which is associated with an increase in upwelling in QBO regions [*Hardiman et al.*, 2007; *Randel et al.*, 2009]. Consequently, during LA the suppressed wave activity is expected to lead to a weaker upwelling in the lower stratosphere. Because the QBO forcing due to upwelling counteracts the stratospheric wave forcing of the QBO, an ad hoc estimate of which mechanism dominates during EL and LA is difficult. Therefore, modeling and observational studies analyze the effect of ENSO on

the QBO. Apart from several studies which do not identify an ENSO signal in the QBO [*Angell*, 1986; *Barnett*, 1991; *Kane*, 1992, 2004], one observational [*Taguchi*, 2010] and one model study [*Calvo et al.*, 2010] show a modulation of the QBO due to ENSO.

The observational study by *Taguchi* [2010] analyzes radiosonde data of monthly mean zonal wind in an empirical orthogonal function (EOF) space following *Wallace et al.* [1993]. The study shows a weaker QBO amplitude during EL compared to during LA conditions, while the westerly phase of the QBO dominates the amplitude reduction. The authors further show a faster QBO downward propagation rate during EL conditions, dominated by the westerly QBO phase. The easterly QBO phase also shows a faster downward propagation rate, but results are statistically insignificant. The observational studies suffer several shortcomings: (i) The chosen EOF method represents the QBO amplitude and the QBO phase propagation in a compact two-dimensional space which allows to apply straightforward statistics. However, this approach also entails disadvantages, because the EOF analysis incorporates an integral value for QBO properties between 10 hPa and the QBO base at ~80 hPa. In this vertical range, both easterly and westerly QBO phases are always simultaneously present. Therefore, the chosen EOF analysis of zonal winds provides an integral value for both easterly and westerly QBO phases. However, the chosen EOF analysis does not allow to relate QBO properties to a certain QBO phase in a clean way, as the authors claim. (ii) The observational record also includes other forcings like volcanic eruptions or long-term solar variability, which does not allow for a clean analysis of the observational record. *Yuan et al.* [2013] extend the work of *Taguchi* [2010], repeating the analysis with a different set of radiosonde data and observing very similar results. Considering the above shortcomings, we summarize only the most sound findings by neglecting the separation into easterly and westerly QBO phases: During EL conditions the QBO amplitude reduces and the QBO downward propagation speed increases, compared to during LA conditions.

The model study by *Calvo et al.* [2010] uses the GCM MAECHAM5, the middle atmosphere configuration of ECHAM5, to perform a 100 year long control run with climatological mean SSTs. Selecting distinct QBO easterly and westerly phases in the control simulation, the authors repeat, for each selected phase, the simulations for 14 months replacing the climatological SSTs with SSTs of the strong El Niño 1997/1998. Combining all easterly and all westerly QBO phases of the control run and the EL runs to an ensemble, the authors find no change in QBO amplitude for both easterly and westerly QBO phases. While the QBO downward propagation rate for the easterly jet shows no change, the QBO downward propagation rate of the westerly jet increases during EL conditions. In a GCM with a GW parameterization, the QBO wave forcing is separated into resolved, large-scale waves and parameterized, smaller-scale gravity waves (GW). The employed model uses a GW parameterization with prescribed and constant GW sources which are not subject to react to the changed tropospheric conditions of El Niño. Thus, the authors attribute the increased downward propagation rate of the westerly jet to an increase in resolved wave activity during EL condition compared to the control run.

Both studies contribute to understanding the effect of ENSO on the QBO but also lack various aspects necessary to deepen our understanding of the presented results. The observational study by *Taguchi* [2010] focuses on the phenomenology of the QBO during ENSO, omitting the physical mechanisms that cause changes in QBO properties. However, observations of stratospheric upwelling and wave activity, with the necessary degree of detail and temporal resolution to explain QBO changes due to ENSO, do not exist. The modeling study by *Calvo et al.* [2010] omits to present the changes in upwelling due to ENSO. Furthermore, the employed GW parameterization includes constant GW sources which do not react to changes of the tropospheric background state, which we observe during ENSO. Finally, the modeling study only compares a single El Niño event with a climatological mean, omitting the effect of La Niña conditions.

In this work, we present results from a model study which includes an analysis of all three QBO-driving mechanisms of a GCM in a comprehensive experimental setup. We first show changes due to ENSO (i) in the resolved waves, (ii) in the parameterized waves, which are physically based in this study, and (iii) in the upwelling in a comprehensive, idealized model framework. In a systematic way, we further analyze the changes of two distinct phases of the QBO to EL and LA conditions. We choose, for the first time, a comprehensive approach to show how changes of all QBO-driving mechanisms, due to ENSO, affect the QBO.

2. Experimental Setup

Isolating the ENSO signal on the QBO in a long time series of data can include cumbersome statistics, because (i) individual ENSO events differ in strength and spatial extent; (ii) any other perturbation or internal variability of the climate system can also affect both the QBO and ENSO and disguise the full ENSO signal on the QBO; (iii) selecting specific ENSO events in such a time series will give a variety of QBO phases, which does not allow for a systematic statistical analysis. We, therefore, use two ensembles, each with a different QBO phase, which react to pronounced SST perturbations due to each El Niño (EL) and La Niña (LA) conditions.

We use the GCM ECHAM6 [*Stevens et al.*, 2013] in a setup as described in *Schirber et al.* [2014a] which includes a physically based GW parameterization for convective GW sources [*Beres et al.*, 2004]. The GW source parameterization launches waves based on the background wind and convective heating properties. The model with this experimental setup produces a QBO with realistic features, [*Schirber et al.*, 2014a]. We perform atmosphere-only simulations with Atmospheric Model Intercomparison Project boundary conditions following *Taylor et al.* [2012]. In order to achieve a clean and pronounced ENSO signal, we select the strongest EL and LA events of the past decades and construct a SST and sea ice concentration (SIC) composite of the detrended observed SST and SIC time series. The EL composite consists the years 1972/1973, 1982/1983, and 1997/1998, and the LA composite includes the years 1955/1956, 1973/1974, 1975/1976, and 1988/1989. We subjectively select the chosen ENSO events on the basis of several ENSO indices with the aim to gain a strong EL and LA signal from more than just a single event. Note that the robustness of the SST signal associated with the EL and LA composite is insensitive to the exact choice of selected events. The composites cover a period of 18 months, from 1 July of the first year until the end of the second year. Because the ENSO signal peaks in boreal winter, the chosen period covers a full cycle of an ENSO perturbation with near neutral ENSO conditions at the start and at the end of the period. We run the experiments with atmospheric boundary conditions and solar irradiance from the year 1988/1989. Even though the ENSO signal is most pronounced in the Pacific, we compile the composite for global SSTs and SICs, including possible teleconnections in regions other than the central Pacific.

We generate two ensembles of each 10 members selected from a pool of each 30 simulations generated with different boundary conditions. The two ensembles constitute an easterly and a westerly QBO phase, which each respond to EL and LA boundary conditions starting from 1 July. In detail, we generate the two ensembles with two different QBO initial conditions as follows, illustrated also in Figure 1. Starting from a single initial QBO profile on 1 January, the QBO evolves independently for each year between 1979 and 2008 for 6 months. The initially identical QBO evolves under different boundary conditions for the first 6 months of each year which leads to different QBO profiles on 1 July. From the pool of 30 QBO profiles on 1 July, we draw 10 profiles with similar QBO amplitude and similar positions of the onset of the jets. We perform this process twice. For each QBOW and QBOE, a different initial profile on 1 January is the basis to draw the members of the QBOW and QBOE ensembles on 1 July. In one case, the initial QBO profile on 1 July exhibits a westerly QBO jet above 10 hPa and an easterly jet below 10 hPa (QBOW). In the second case the easterly jet is positioned above the westerly jet which prevails below 10 hPa (QBOE). For the detailed wind profiles of QBOW, see the initial profile of Figure 6 and for QBOE see Figure 9. For all analysis and figures in this chapter except Figure 5, we compute the meridional mean between −10° and +10° latitude.

Summarizing the experimental setup, we run the four different types of simulations shown in Table 1: Having generated two 10 member ensembles of a QBOW and a QBOE initial wind profile on 1 July, we run both ensembles for each EL and LA boundary conditions lasting 18 months. The chosen experimental setup aims at isolating the effect of the difference between EL and LA on the QBO. Considering the oscillatory character of the QBO, we analyze the ENSO effect on two QBO phases, QBOW and QBOE.

3. Changes in the Background State

3.1. Surface Temperature and Precipitation

Before showing the forcing quantities relevant for the QBO, we show how ENSO modulates physical quantities in the troposphere. Although the ENSO signal peaks in the Pacific, we show the mean along the entire equator because the amount of waves in the entire tropics, and not the waves in any specific area, drive the QBO. Considering the entire tropics, we furthermore include possible teleconnections related to ENSO. The temperature at 2 m closely follows the SSTs. During EL conditions, the temperature at 2 m is

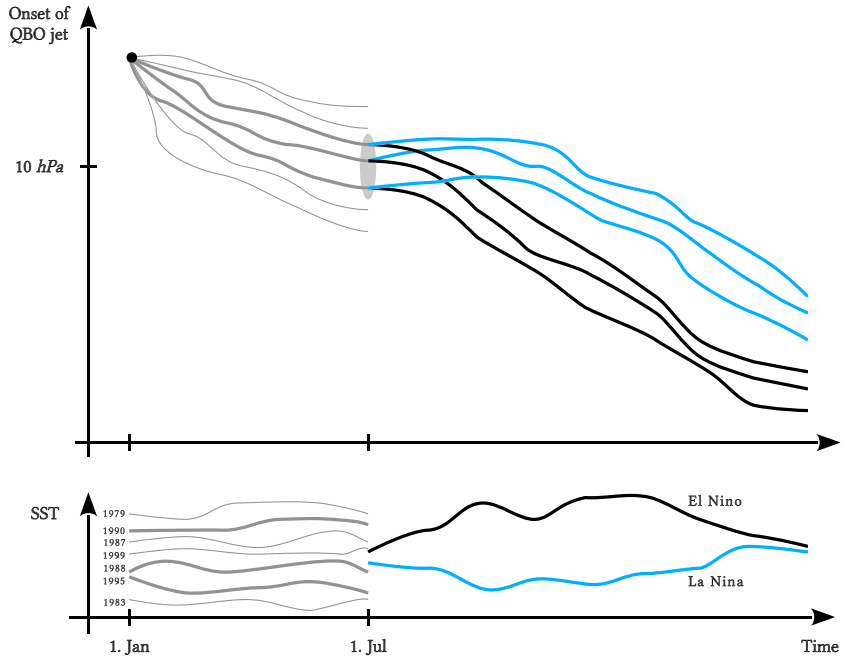

Figure 1. Illustration of the experimental setup. First part of the time axis until 1 July shows the generation of an ensemble with similar QBO characteristics (thick gray), the second part of the time axis after 1 July shows how the same ensemble reacts differently to EL (black) and LA (blue) conditions. (top) The position of the onset of the QBO jet, valid for both the easterly and the westerly jets, (bottom) the different SSTs to generate the ensemble and the different SSTs during EL and LA. The actual ensemble comprises 10 members, not three as illustrated in the figure, and the actual number of model runs from which the ensemble is drawn is 30, not seven as illustrated in the figure.

generally higher than during LA conditions, while the difference peaks with 1.5 K at December and January, see Figure 2 (left). Since we prescribe the SSTs for EL and LA conditions, the ensemble spread in the 2 m temperature is small, possibly related to variability in the large-scale circulation over land.

The amount of precipitation is closely linked to the surface temperatures, see Figure 2 (right). The total precipitation during EL exceeds the precipitation during LA, with a mean increase of ∼ 25% during EL compared to LA between October and March. Since the convective precipitation exceeds the large-scale precipitation at the equator by a factor ∼ 30 (not shown), the convective precipitation dominates the changes in total precipitation between EL and LA conditions. The increase in precipitation is closely linked to the amount of convective heating which in turn governs the amplitudes of the excited waves, see *Schirber et al.* [2014a] for GWs. We, therefore, expect the increase in precipitation during EL to project on the amount of excited waves, presented in the next chapter.

The model results agree with observation which also show an increase in precipitation rate with an increase in tropical SSTs. Regressing tropical precipitation rates from the microwave sounding unit with SST anomalies in a 10 year time series, *Soden* [2000] find a regression coefficient of 0.77 mm/d/K. Using this regression coefficient, a peak difference of ∼ 1.5 K between EL and LA conditions gives an increase in precipitation rate of ∼ 1.2 mm/d. This simple calculation agrees with the modeled peak increase in precipitation rate of ∼ 1.4 mm/d.

Note that other observational studies do not identify a relationship between ENSO and equatorial global mean precipitation. *Gu et al.* [2007] analyze the time series of Global Precipitation Climatology Project and do not find an ENSO signal in the precipitation. However, two of the three strongest El Niño events in this time series, according to the Niño 3.4 index, coincide with the volcanic eruptions El Chichón (1982/1983) and Pinatubo (1991/1992). Volcanic eruptions suppress

Table 1. Overview of Number of Ensemble Members for the Experimental Setup With Two Initial QBO Phases (QBOW and QBOE) and Two Different ENSO Boundary Conditions (El Niño and La Niña)

	QBOW	QBOE
El Niño	#10	#10
La Niña	#10	#10

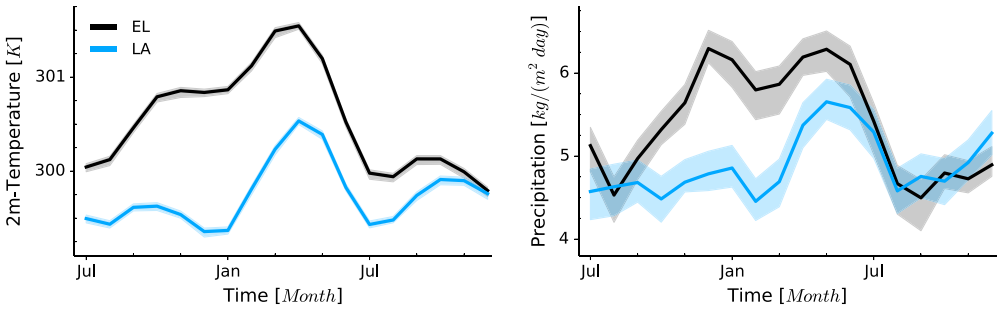

Figure 2. Time series of zonal and meridional (left) mean temperature at 2 m and (right) precipitation for El Niño (black) and La Niña (blue) conditions during QBOE phase. Temperature at 2 m and precipitation for QBOW phase (not shown) are qualitatively similar to QBOE phase. The shown precipitation is the sum of parameterized, convective precipitation and resolved, large-scale precipitation. Solid lines show the ensemble means, and shading indicates the range of 2 standard deviations (2σ).

precipitation and therefore oppose the suggested increase in tropical precipitation during El Niño events [*Gu et al.*, 2007]. The fact that volcanic eruptions dominate the variability in the observed time series of tropical precipitation in their analysis may explain why *Gu et al.* [2007] present different results than *Soden* [2000].

3.2. Wave Activity and Upwelling

Before presenting changes in wave activity and upwelling, we clarify the employed terminology. We relate the term "QBO forcing" to the general processes that act on the QBO, such as the resolved waves, the parameterized waves and the tropical upwelling in the stratosphere. We do not relate the term "QBO forcing" to the tendency of zonal wind $\frac{\partial U}{\partial t}$ which actually acts on the QBO and causes the downward propagation of the QBO. Because the tendency components also depend on the QBO amplitude, we cannot unambiguously assign changes in the tendency components to changes in the forcing if the QBO amplitude changes simultaneously, see also the discussion in section 5. We therefore relate "QBO forcing" to the general process causing the change in tendency. In detail, we relate "QBO forcing" to physical quantities expressing the general process, such as momentum flux B for gravity waves, the vertical component F_z of the Eliassen-Palm (EP) Flux vector for resolved waves and the vertical velocity w^* of a transformed Eulerian mean analysis for the increase in the tropical branch of the Brewer-Dobson circulation, i.e., the upwelling.

The amount of the resolved waves increases during EL compared to LA. We use the vertical component F_z of the EP flux vector as a proxy for resolved wave activity [*Andrews et al.*, 1987]. We compute the EP flux in wave number-frequency space after *Horinouchi et al.* [2003] based on 6 hourly instantaneous values. Note that wave activity, and the wind tendency on the QBO, associated with the meridional component F_y is comparable in strength to the vertical component F_z, but plotting F_y is not feasible for visualization because

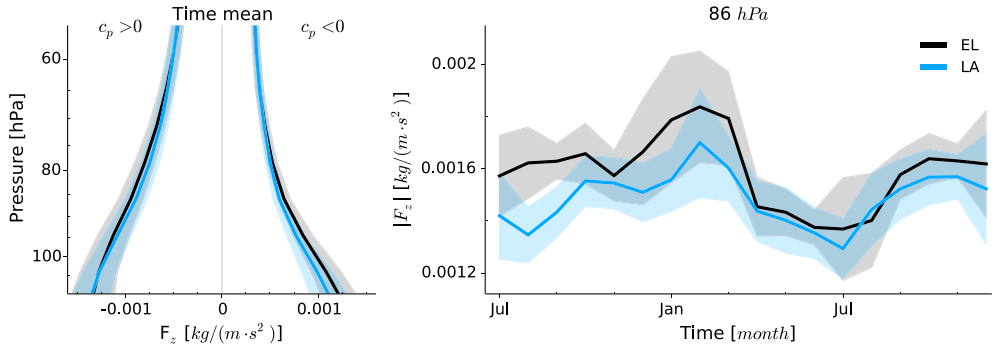

Figure 3. Vertical component F_z of the spectral EP-Flux vector for El Niño (black) and La Niña (blue) conditions during QBOE phase. Vertical EP-Flux vector F_z for QBOW phase (not shown) is qualitatively similar to QBOE phase. Meridional mean of F_z, scaled by density ρ, shows the integral overall frequencies and wave numbers. Solid lines show the ensemble means, and shading indicates the range of 2 standard deviations (2σ). (left) Vertical profile of time mean F_z for westward ($c < 0$) and eastward ($c > 0$) waves. (right) Time series of absolute $|F_z|$ at 86 hPa, with $|F_z| = |F_{z,c<0}| + |F_{z,c>0}|$.

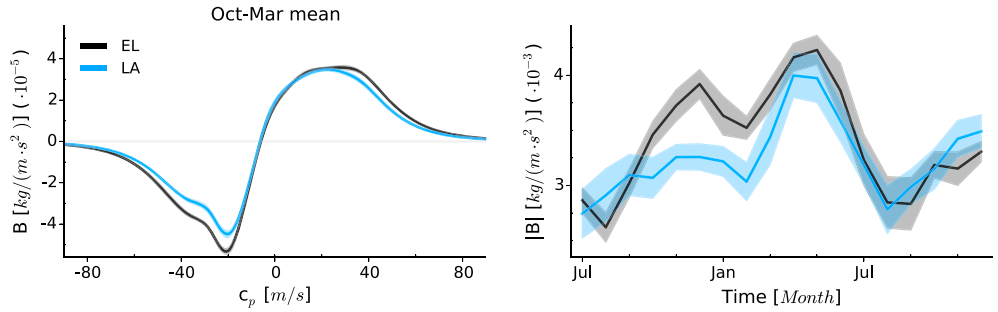

Figure 4. GW source momentum flux *B* for El Niño (black) and La Niña (blue) conditions during QBOE phase. GW source momentum flux *B* for QBOW phase (not shown) is qualitatively similar to QBOE phase. Zonal and meridional mean of *B*, scaled by density ρ, is determined at the top of convection. Solid lines show the ensemble means and shading indicates the range of 2 standard deviations (2σ). (left) Source spectrum of *B* as a function of horizontal phase speed c_p, time mean between October and March. (right) Time series of total amount of source momentum flux $|B|$ integrated over c_p.

the sign of F_y changes continuously with the sign of the background wind. The amount of momentum carried by resolved waves decreases continuously as waves travel upward and dissipate, see Figure 3 (left). During EL, the profiles of F_z increase for both westward ($c_p < 0$) and eastward ($c_p > 0$) waves on an 18 months time mean. We omit extending the profile above 55 hPa because the different evolution of the QBO jets above will cause different wave filtering and therefore does not allow to compare the profiles. The time series of the sum of westward and eastward waves associated with F_z at 86 hPa, just below the QBO region, shows higher values of momentum fluxes, peaking in December-January-February, for EL compared to LA conditions. Note that the 2 σ ranges of the EL and LA time series overlap in large parts.

The amount of the parameterized gravity waves responds to the presented changes in tropospheric quantities and increases during EL compared to LA. The mean source spectrum shows an increase in momentum flux between −60 m/s and −10 m/s phase speed in the westward waves, and an increase between 20 m/s and 60 m/s phase speed in the westerly waves, see Figure 4 (left). The increase of momentum fluxes at large phase speeds is caused by an increase in the vertical extent of convection. The deepening of convection during EL is in line with higher surface temperatures and increased precipitation [*Schirber et al.*, 2014b]. Note that in the chosen GW parameterization setup, momentum fluxes at large horizontal phase speeds also break in QBO relevant heights. This may be unrealistic and is an effect of compensating deficiencies in the shape of the GW source spectrum, for more details see *Schirber et al.* [2014a]. The time series of the total amount of source momentum flux $|B|$ (with $B = \rho \cdot \overline{u'w'}$) follows, to a first approximation, the time series of precipitation, compare Figure 2 (right) with Figure 4 (right). The amount of source momentum flux *B* scales with the amount of convective heating Q_0, with $B \propto Q_0^2$. An increase in precipitation is associated with an increase in the amount of convective heating Q_0 and, therefore, an increase in the amount of excited source momentum flux *B*. For more details on the physical link of GWs to the sources, see *Beres et al.* [2004] and

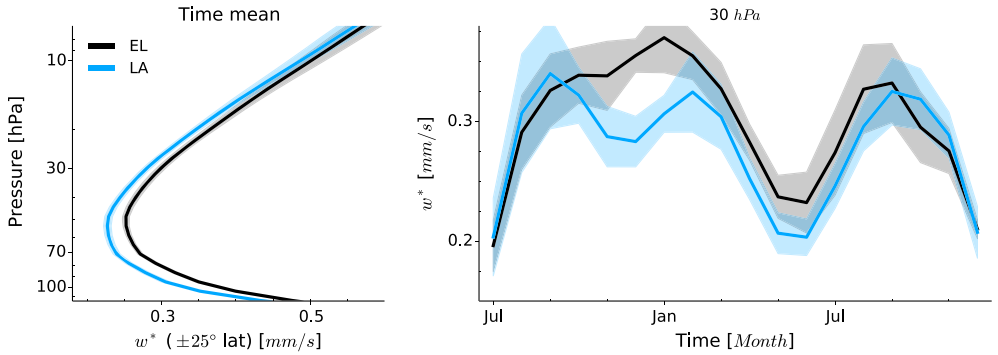

Figure 5. Upwelling w^* for El Niño (black) and La Niña (blue) conditions during QBOE phase. Upwelling w^* for QBOW phase (not shown) is qualitatively similar to QBOE phase. Zonal and meridional mean between −25° and +25° latitude. Solid lines show the ensemble means, and shading indicates the range of 2 standard deviations (2σ). (left) Vertical profile of time mean. (right) Time series at 30 hPa.

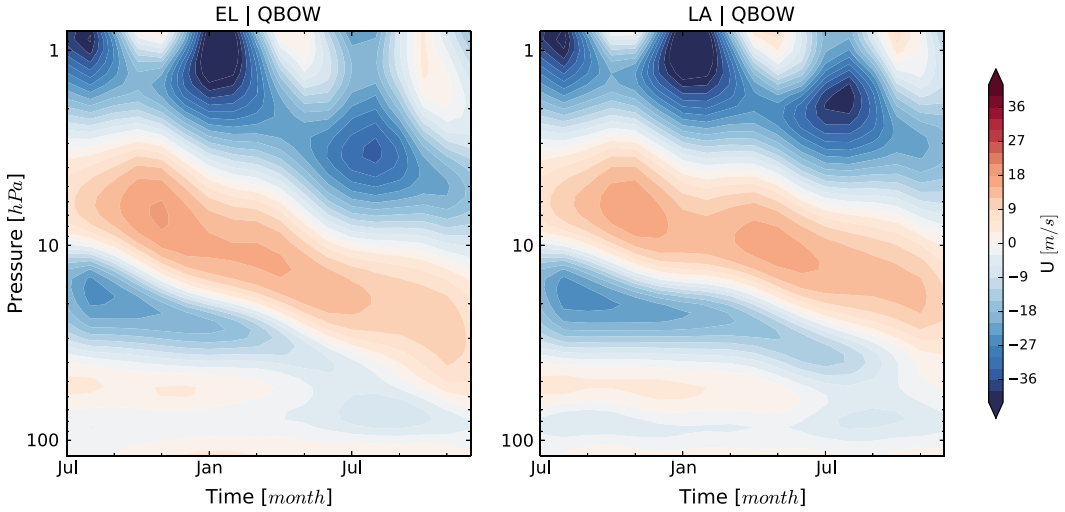

Figure 6. Evolution of the QBO for (left) El Niño and (right) La Niña conditions during QBOW phase. Time series of the profile of meridional and zonal mean zonal wind *U* for the ensemble mean.

Schirber et al. [2014a]. The total source momentum flux during EL is bigger than during LA conditions, with a mean increase of ∼15% during EL compared to LA between October and March.

Both resolved and parameterized waves show an increase in wave activity, and also the upwelling w^* in the QBO region increases during EL compared to LA. The vertical profile of upwelling is positive, and therefore directed upward, throughout the lower stratosphere with a minimum around 50 hPa, see Figure 5 (left). During EL conditions, we see a general shift to higher values, independent of the height of the profile. The time series at 30 hPa shows a strong annual cycle with a minimum in early boreal summer, see Figure 5 (right). During EL conditions, the upwelling increases compared to LA conditions, showing the largest effect around the first boreal winter in the time series, in accordance with the strongest difference in ENSO signals and the strongest difference in wave activity.

4. Evolution of Two QBO Phases

As outlined in the experimental setup, we analyze the effect of EL and LA conditions on the QBO by selecting two phases of the QBO which oppose each other in the position of the jets. We first present results for QBOW, followed by QBOE, before we discuss the results in the subsequent chapter.

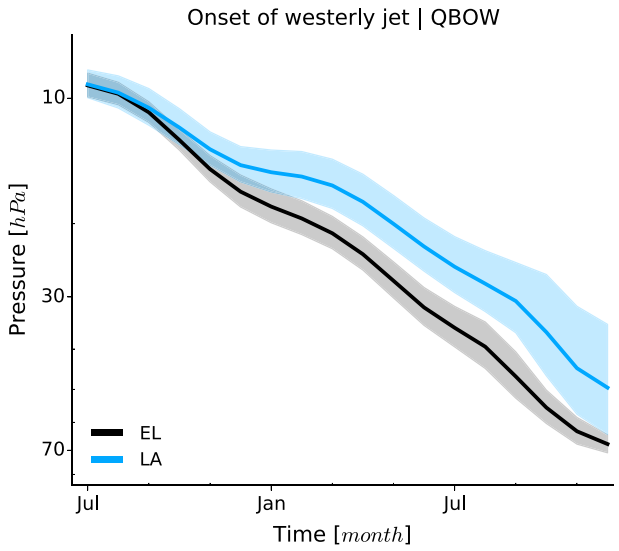

Figure 7. Time series of the onset of the westerly jet in QBOW for El Niño (black) and La Niña (blue) conditions. Solid lines show the ensemble means, and shading indicates the range of 2 standard deviations (2σ).

4.1. QBOW

The initial wind profile of QBOW contains the onset of a westerly jet at around 10 hPa with westerly winds above. Below 10 hPa, the underlying easterly jet extends until 40 hPa, where the remainder of a previous westerly phases resides, see initial profile in July in Figure 6. Note that the remainder of the westerly jet at 50 hPa at this phase of the QBO is stronger than reanalysis product suggests [*Schirber et al.*, 2014a]. In the course of the simulation period, the westerly jet above 10 hPa slowly descends through the lower stratosphere. In the course of the

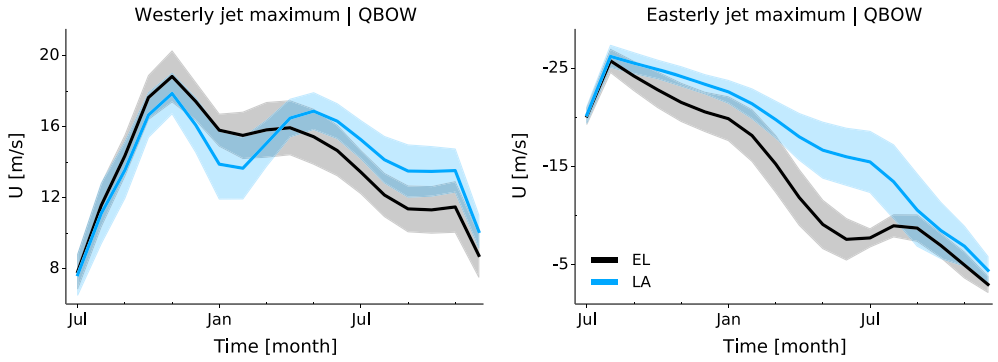

Figure 8. Time series of the strength of the (left) westerly and (right) easterly jets of QBOW for El Niño (black) and La Niña (blue) conditions. Solid lines show the ensemble means, and shading indicates the range of 2 standard deviations (2σ).

simulation, the easterly jet below 10 hPa descends and slowly erases the underlying westerly jet, which persists longer during LA conditions. Centered around 1 hPa above the main QBO region, the semiannual oscillation (SAO) shows its periodic change of winds with a period of 6 months. In the following, we present two characteristic QBO quantities, the downward propagation of the QBO westerly jet and the strength of QBO jets, and compare these quantities during EL and LA conditions.

The downward propagation rate illustrates the speed of how quickly the QBO jets descend in time. We determine the onset of the westerly jet and track the vertical position in time, see Figure 7. At the end of the simulation period of 18 months, the westerly jet reaches 70 hPa during EL, while the onset of the westerly jet resides at 50 hPa during LA conditions. During EL conditions, the QBO westerly jet therefore descends faster than during LA conditions. Note that the 2σ ranges of the ensemble do not intersect for most parts, indicating a robust difference between EL and LA conditions.

We analyze the strength of the QBO jet by determining the maximum wind speed within the westerly and the easterly jet and track the maximum values in time. The westerly jet, whose position is close to the SAO in the upper stratosphere, exhibits a semiannual signal in jet strength, see Figure 8 (left). While the strength of the westerly jet is slightly stronger during EL conditions in the first half of the simulation period, the jet strength is weaker during EL conditions in the second half of the simulation period, compared to LA conditions. The strength of the easterly jet decreases in the course of the simulation during both EL and LA conditions, while the strength of the easterly jet is generally weaker during EL conditions compared to during LA conditions, see Figure 8 (right).

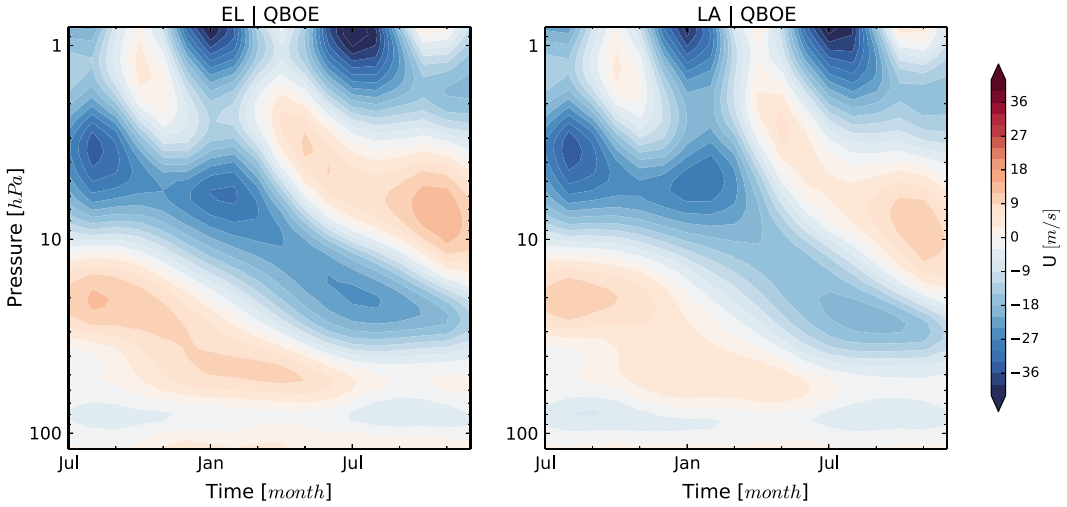

Figure 9. Evolution of the QBO for (left) El Niño and (right) La Niña conditions during QBOE phase. Time series of the profile of meridional and zonal mean zonal wind *U* for the ensemble mean.

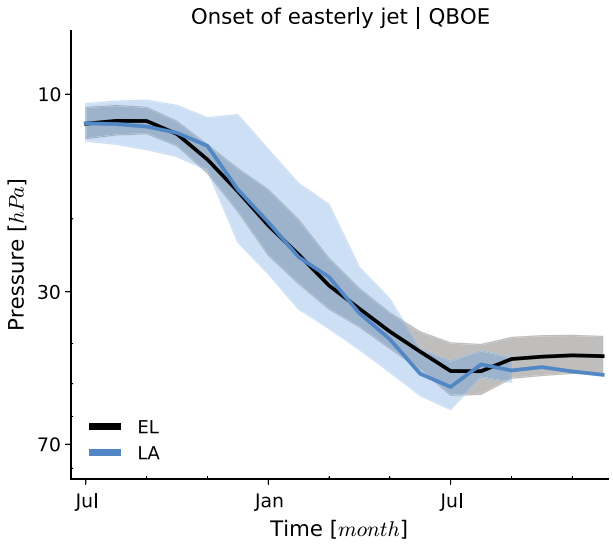

Figure 10. Time series of the onset of the easterly jet in QBOE for El Niño (black) and La Niña (blue) conditions. Solid lines show the ensemble means, and shading indicates the range of 2 standard deviations (2σ). Note that the ensemble consists of only one member during the last months of LA.

4.2. QBOE

The initial wind profile of QBOE opposes the QBOW profile, with an easterly jet above 10 hPa and a westerly jet below, see initial profiles of Figure 9. In the course of the experiment, both the easterly and the westerly jets descend through the lower stratosphere while the descending easterly jet eventually terminates the westerly jet in boreal summer of the second year. The downward propagation of the easterly jet is similar for both EL and LA conditions, see Figure 10. However, the ensemble spread increases strongly during LA conditions coinciding with the onset of the strong ENSO signal in early boreal winter. Finally, the strength of the QBO westerly jet clearly decreases during LA conditions compared to EL conditions; see Figure 11. While the strength of the westerly jet compares well for LA and EL conditions during the first part of the simulation period, the strength of the easterly jet decreases for LA compared to EL in the second part of the simulation.

5. Wind Tendencies of Different QBO Forcing Mechanisms

We briefly summarize the preceding results which serve as the basis for the following discussion. During EL conditions, wave activity increases, which on one hand increases the QBO forcing due to waves and on the other hand increases the tropical upwelling which counteracts QBO forcing due to waves. We, therefore, observe an increase in two opposing QBO forcings in EL compared to LA conditions. The changes in QBO forcing due to EL and LA act on both QBOW and QBOE, yet the jets of QBOW and QBOE react differently: On one hand, the westerly jet of QBOW descends quicker, Figure 7, and the underlying easterly jet below the westerly jet is weaker during EL, in Figure 8 (right). On the other hand, the easterly jet of QBOE descends with similar speed during EL and LA, Figure 10, and the underlying westerly jet is stronger during EL, Figure 11 (left).

In order to illustrate the sometimes limited informative value of comparing tendency profiles of different QBOs, we show tendency profiles for the month of May in the second year for the QBOE initial condition.

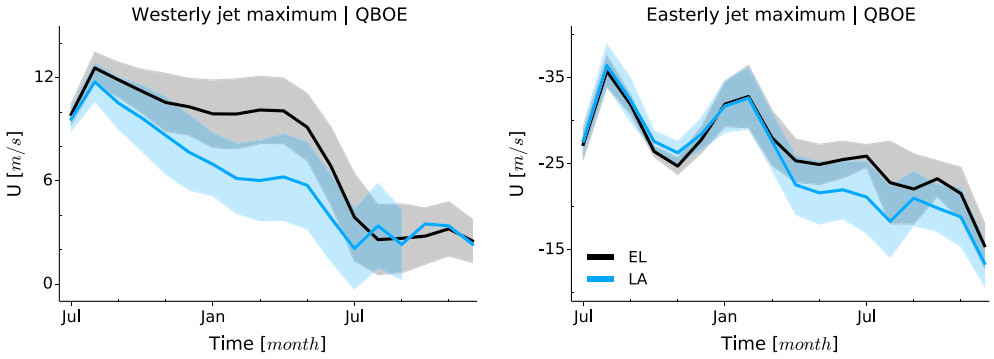

Figure 11. Time series of the strength of the (left) westerly and (right) easterly jets of QBOE for El Niño (black) and La Niña (blue) conditions. Solid lines show the ensemble means, and shading indicates the range of 2 standard deviations (2σ). Note that the ensemble for the westerly jet consists of only one member during the last months of LA.

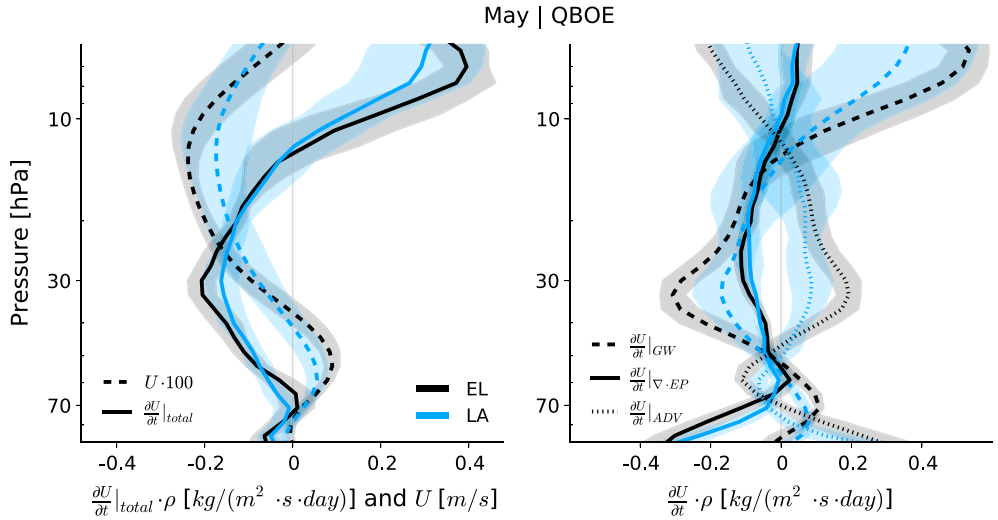

Figure 12. Vertical profile of zonal wind U and its tendency $\frac{\partial U}{\partial t}$ for QBOE in May of the second year for El Niño (black) and La Niña (blue) conditions. Lines show the ensemble means, and shading indicates the range of 2 standard deviations (2σ). (left) Zonal wind (dashed), scaled by a factor 100, and total tendency $\frac{\partial U}{\partial t}|_{\text{total}}$ (solid). (right) Tendency components of resolved waves $\frac{\partial U}{\partial t}|_{\nabla \cdot \text{EP}}$ (solid), gravity waves $\frac{\partial U}{\partial t}|_{\text{GW}}$ (dashed), and advection $\frac{\partial U}{\partial t}|_{\text{ADV}}$ (dotted).

At this time, the QBO under EL and LA has evolved in the course of the experiment and shows a different wind profile for EL and LA conditions. While the onset of the westerly jet coincides at ~40 hPa for both EL and LA conditions, the amplitude of the jets differs; see Figure 12 (left). The total tendency $\frac{\partial U}{\partial t}|_{\text{total}}$ for EL exceeds LA conditions, and the larger tendency for EL is consistent with the identical downward propagation speed for EL and LA. In order to descend with a similar speed, the QBO in EL with stronger amplitude requires more tendency than the QBO in LA with a weaker amplitude. The individual tendency profiles, which add up to the total tendency, each differs under EL and LA conditions; see Figure 12 (right). While the wind tendency due to GWs $\frac{\partial U}{\partial t}|_{\text{GW}}$ and the tendency due to advection $\frac{\partial U}{\partial t}|_{\text{ADV}}$ change by about a factor 2, the tendency due to the resolved wave $\frac{\partial U}{\partial t}|_{\nabla \cdot \text{EP}}$ increases only slightly during EL compared to LA conditions. Since in this case, both the background wind and the QBO forcing mechanisms differ at the same time, we cannot identify the contribution of either of the two causes to changes in the tendency profile.

Having pointed out the limitations of an analysis of QBO tendency profiles, we nevertheless can deduce informative value from tendency profiles of QBOs, if the QBOs exhibit a similar wind structure. For both QBOW and QBOE, we choose the onset of the ENSO signal in October of the first year, 4 months after the start of the simulation, to compare tendency profiles of EL and LA conditions. Even though the ENSO signal peaks later in time, and the difference in QBO forcing would then be strongest, we choose the onset of the ENSO signal because the QBO profiles are still similar in October of the first year. At a later point in time, the wind profiles differ strongly and do not allow for sound reasoning as pointed out in the previous paragraph. Note that choosing a month earlier or later than October shows qualitatively similar results, but the signal is not as pronounced due to the above mentioned shortcomings.

5.1. QBOW

In October, the onset of the westerly jet of QBOW is situated at ~15 hPa with an easterly jet below; see Figure 13 (left). The profiles under EL and LA conditions still show comparable characteristics but differ already. The onset of the westerly jet is lower during EL conditions than during LA conditions. As a consequence, also the profile of the total tendency $\frac{\partial U}{\partial t}|_{\text{total}}$ peaks at a lower position during EL than during LA conditions. However, also the peak value during EL exceeds the peak value during LA conditions, which we do not associate with the slightly lower westerly jet, but with a change in QBO forcing. The change in the total tendency is caused by the resolved waves $\frac{\partial U}{\partial t}|_{\nabla \cdot \text{EP}}$ and the parameterized waves $\frac{\partial U}{\partial t}|_{\text{GW}}$; see Figure 13 (right). While the exerted acceleration increases for both wave components during EL, the tendency due to advection $\frac{\partial U}{\partial t}|_{\text{ADV}}$ only changes the vertical position, following the lower position of the wind profile in EL, but does not change its peak value.

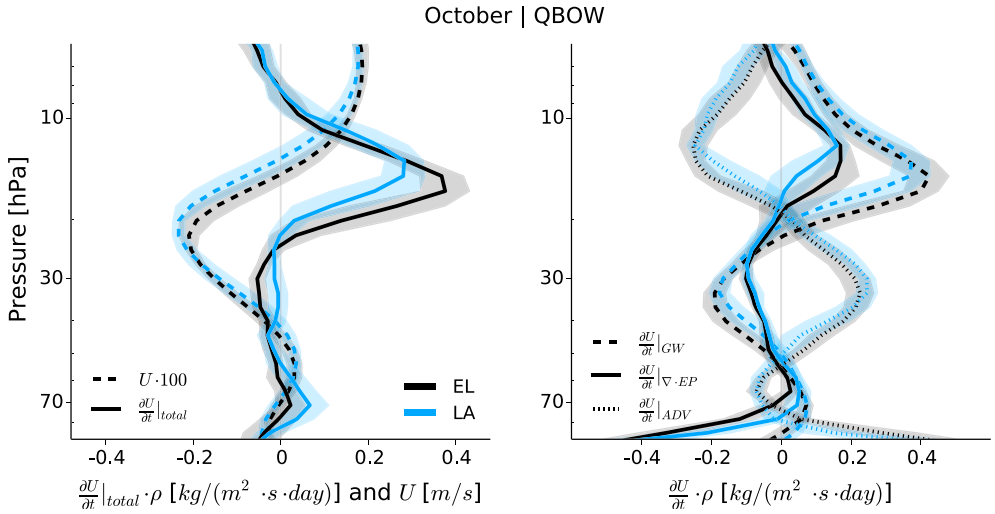

Figure 13. Same as Figure 12 but for October of the first year instead of May of the second year and for QBOW instead of QBOE.

We conclude from this analysis that the increase in wave forcing, as described in chapter 3.2, exerts more acceleration and therefore leads to a quicker downward propagation of the westerly jet during EL conditions, compared to LA conditions. We base this conclusion on findings which show that the amount of exerted acceleration correlates with the speed of the QBO jet downward propagation [*Scaife et al.*, 2000; *Schirber et al.*, 2014a]. We do not detect any signal of the observed increase in upwelling in the tendency profile. In addition, the strength of the underlying easterly jet weakens in the course of the experiment for EL compared to LA conditions; see Figure 8 (right). The westerly jet has to erode the underlying easterly jet, before the westerly jet can descend. During EL, a weaker easterly jet requires less momentum to be eroded and therefore favors a quicker downward propagation of the westerly jet above. Summarizing the two aspects, the increase in wave forcing and the weaker easterly jet, lead to a quicker downward propagation of the westerly jet during EL compared to LA conditions.

5.2. QBOE

In October, the QBO tendency profile for QBOE shows similar characteristic changes during EL as for QBOW. For QBOE in October, the easterly jet above ~15 hPa is situated above a westerly jet which extends down to 70 hPa, see Figure 14 (left). The total tendency increases during EL compared to LA, along with a lower peak in the GW component in agreement with the slightly lower position of the onset of the easterly jet during EL. As for QBOW, both wave components, dominated by the GWs, cause the increase in total tendency while the tendency due to advection remains unchanged in strength; see Figure 14 (right).

Following the previously presented argumentation that increased total tendency leads to a quicker downward propagation of the QBO jet, we would expect a faster downward propagation speed of the easterly jet in QBOE. However, we observe no change in downward propagation speed of the easterly jet in QBOE during EL compared to LA conditions; see Figure 10. We explain this apparent discrepancy by considering the second aspect that also controls the downward propagation speed, which is the strength of the underlying jet. While for QBOW the underlying easterly jet is weaker during EL, the underlying westerly jet in QBOE is stronger during EL, see Figure 11 (left). While a relatively weaker underlying jet favors a faster downward progression of the above jet, a relatively stronger underlying jet inhibits a faster downward propagation of the above jet.

For QBOE, we conclude that the increase in wave forcing, and therefore the increase in exerted acceleration, is balanced by the increase in the underlying jet strength during EL compared to LA conditions. The changes of the two opposing mechanisms cancel each other which leads to no changes in the downward propagation of the easterly jet during EL and LA conditions. For QBOW in contrast, the weaker underlying jet, in addition to an increase in wave forcing, both favor a faster downward propagation speed of the jet.

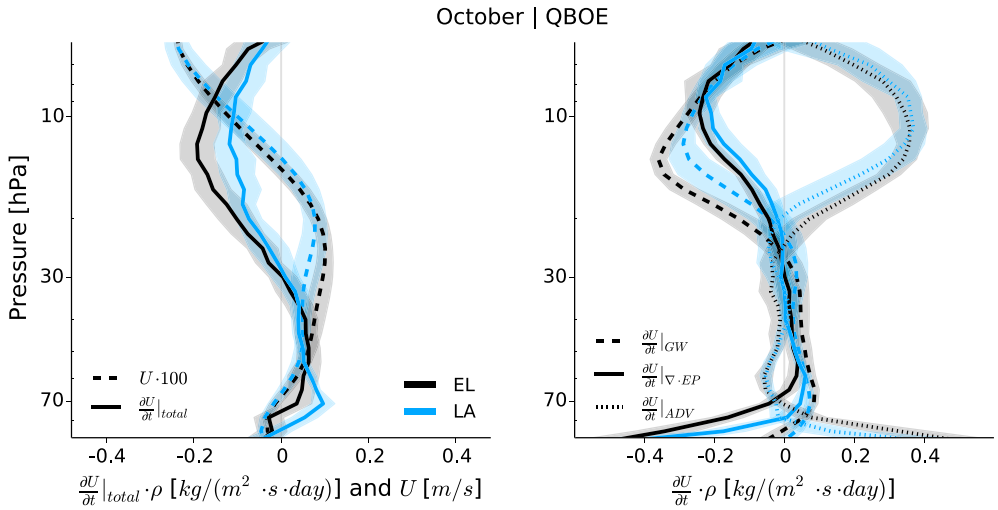

Figure 14. Same as Figure 12 but for October of the first year instead of May of the second year.

6. Summary and Conclusion

6.1. Summary

In an idealized experimental setup, we generate two ensembles, each containing 10 members, with opposing QBO initial conditions. While QBOW includes a westerly jet above 10 hPa and an easterly jet below, QBOE contains an easterly jet above 10 hPa and a westerly jet below. In atmosphere-only simulations, both QBOW and QBOE ensembles experience El Niño (EL) and La Niña (LA) boundary conditions, which we composite from observed SST of particularly strong El Niño and La Niña events of the last decades. We compare the evolution of the two QBO phases, QBOW and QBOE, under the two different boundary conditions of EL and LA to isolate the effect of ENSO on the QBO. See Figure 1 for an illustration of the ensemble generation and the experimental setup.

During EL conditions, the globally higher SSTs and the associated increased tropospheric convections are a manifestation of an increase in wave activity. Stronger wave activity has two opposing effects on the net QBO forcing. On one hand, an increase in tropospheric wave activity, the main QBO forcing, leads to stronger QBO forcing. On the other hand, stronger wave activity leads to an intensification of the tropical upwelling in the lower stratosphere, which counteracts QBO wave forcing. While studies show an increase in upwelling during EL [*Hardiman et al.*, 2007; *Randel et al.*, 2009], *Ortland and Alexander* [2014] show in detail that increased wave activity in the tropics increases upwelling in the lowermost stratosphere.

The ENSO signal of EL and LA causes differences in QBO behavior, depending on the initial condition of the QBO. During EL, the westerly jet in QBOW descends faster and the underlying easterly jet is weaker than during LA conditions. The easterly jet in QBOE descends with similar speed during both EL and LA conditions, while the underlying westerly jet is stronger during EL compared to LA. An analysis of the zonal wind tendency profile helps to explain the results. The increase in total tendency at the beginning of the ENSO signal shows an increase in the tendency due to both resolved and parameterized waves. Despite the stronger diagnosed upwelling, the tendency due to advection does not change, indicating that changes in upwelling are of second-order importance compared to changes in the QBO amplitude and therefore the secondary circulation of the QBO.

The presented results agree with findings of *Calvo et al.* [2010], who show no change in QBO downward progression speed for the easterly jet, but observe a faster downward progression during EL for the westerly jet. Furthermore, *Calvo et al.* [2010] observe no change in amplitude in both the easterly and the westerly jets during EL conditions. This also agrees with our results which do not show any systematic change in amplitude of the upper QBO jets. We cannot compare our results with the observational study of *Taguchi* [2010] in a detailed way, since the authors use vertically integrated values of QBO quantities including both the upper and the lower QBO jet. However, *Taguchi* [2010] also finds a faster downward propagation speed during EL, dominated by the westerly jet. Apart from confirming findings of previous studies on the

influence of ENSO on the QBO, we further show the mechanisms and reasons for the observed changes in QBO downward propagation.

Even though we argue in a consistent and physically solid way by considering the effect of the underlying jet on the downward propagation speed, we are not able to explain why the strength of the underlying jet behaves differently for QBOE and QBOW. We do not succeed in identifying a reason or hypothesis for the change in QBO amplitude due to the strong coupling between individual QBO forcings. Additionally, the strong feedbacks between changes in QBO forcing, changes in QBO amplitude, and changes in QBO downward progression in a complex GCM impede a logical chain of argumentation or reasoning.

6.2. Conclusion

ENSO modulates QBO properties. During EL compared to LA, changes in QBO properties are driven by QBO forcings due to resolved and parameterized waves, while changes in upwelling do not contribute significantly. We explain the different behavior in downward propagation speed of the QBO jets in QBOE and QBOW by considering two mechanisms. First, an increase in wave forcing and, second, a weaker underlying jet, both favor a faster downward propagation speed of a QBO jet. During EL, wave activity increases for both QBOE and QBOW and affects the jets in a very similar way at the onset of the ENSO signal. In QBOW, the underlying easterly jet is weaker during EL, while in QBOE the underlying westerly jet is stronger during EL. In QBOW, both the increase in QBO wave forcing and the weaker underlying easterly jet favor a faster downward propagation of the westerly jet. In QBOE, however, the increase in QBO wave forcing is balanced by the stronger underlying westerly, so that the downward propagation speed under EL and LA conditions remains unchanged.

Acknowledgments

The author thanks the Max Planck Society and the International Max Planck Research School for Earth System Modeling. The author thanks Elisa Manzini for providing the initial idea for this work and Thomas Krismer and Elisa Manzini for providing valuable feedback on this manuscript. Simulations were carried out on the supercomputing facilities of the German Climate Computation Centre (DKRZ) in Hamburg. For access to the data, please contact sebastian.schirber@mpimet.mpg.de.

References

Alexander, M., and J. Holton (1997), A model study of zonal forcing in the equatorial stratosphere by convectively induced gravity waves, *J. Atmos. Sci.*, *54*, 408–419.

Andrews, D. G., J. R. Holton, and C. B. Leovy (1987), *Middle Atmosphere Dynamics*, Academic Press, Waltham, Mass.

Angell, J. K. (1986), On the variation in period and amplitude of the quasi-biennial oscillation in the equatorial stratosphere, 1951–85, *Mon. Weather Rev.*, *114*, 2272–2278.

Baldwin, M., et al. (2001), The quasi-biennial oscillation, *Rev. Geophys.*, *39*(2), 179–229.

Barnett, T. (1991), The interaction of multiple time scales in the tropical climate system, *J. Clim.*, *4*, 269–285.

Beres, J. H., M. J. Alexander, and J. R. Holton (2004), A method of specifying the gravity wave spectrum above convection based on latent heating properties and background wind, *J. Atmos. Sci.*, *61*(3), 324–337, doi:10.1175/1520-0469(2004)061<0324:AMOSTG>2.0.CO;2.

Bergman, J., and M. Salby (1994), Equatorial wave activity derived from fluctuations in observed convection, *J. Atmos. Sci.*, *51*(24), 3791–3806.

Calvo, N., M. A. Giorgetta, and C. Pena-Ortiz (2010), Impact of warm ENSO events on the tropical QBO using MAECHAM5 simulations, paper presented at Poster at EGU Conference, EGU General Assembly, Vienna, Austria, 2–7 May.

Gu, G., R. F. Adler, G. J. Huffman, and S. Curtis (2007), Tropical rainfall variability on interannual-to-interdecadal and longer time scales derived from the GPCP monthly product, *J. Clim.*, *20*(15), 4033–4046, doi:10.1175/JCLI4227.1.

Hardiman, S. C., N. Butchart, P. H. Haynes, and S. H. E. Hare (2007), A note on forced versus internal variability of the stratosphere, *Geophys. Res. Lett.*, *34*, L12803, doi:10.1029/2007GL029726.

Horinouchi, T., et al. (2003), Tropical cumulus convection and upward-propagating waves in middle-atmospheric GCMs, *J. Atmos. Sci.*, *60*(22), 2765–2782, doi:10.1175/1520-0469(2003)060<2765:TCCAUW>2.0.CO;2.

Kane, R. (1992), Relationship between QBOs of stratospheric winds, ENSO variability and other atmospheric parameters, *Int. J. Climatol.*, *12*, 435–447.

Kane, R. P. (2004), Comparison of stratospheric zonal winds and El Niño-Southern Oscillation in recent decades, *Int. J. Climatol.*, *24*(4), 525–532, doi:10.1002/joc.1004.

Lindzen, R., and J. Holton (1968), A theory of the quasi-biennial oscillation, *J. Atmos. Sci.*, *25*, 1095–1107.

Ortland, D. A., and M. J. Alexander (2014), The residual-mean circulation in the tropical tropopause layer driven by tropical waves, *J. Atmos. Sci.*, *71*(4), 1305–1322, doi:10.1175/JAS-D-13-0100.1.

Pfister, L., S. Scott, M. Lowenstein, S. Bowen, and M. Legg (1993), Mesoscale disturbances in the tropical stratosphere excite by convection: Observations and effects on the stratospheric momentum budget, *J. Atmos. Sci.*, *50*(8), 1058–1075.

Randel, W. J., R. R. Garcia, N. Calvo, and D. Marsh (2009), ENSO influence on zonal mean temperature and ozone in the tropical lower stratosphere, *Geophys. Res. Lett.*, *36*, L15822, doi:10.1029/2009GL039343.

Scaife, A., N. Butchart, C. D. Warner, D. Stainforth, W. Norton, and J. Austin (2000), Realistic quasi biennial oscillations in a simulation of the global climate, *Geophys. Res. Lett.*, *27*(21), 3481–3484.

Schirber, S., E. Manzini, and M. J. Alexander (2014a), A convection based gravity wave parameterization in a general circulation model: Implementation and improvements on the QBO, *J. Adv. Model. Earth Syst.*, *6*, 264–279, doi:10.1002/2013MS000286.

Schirber, S., E. Manzini, T. Krismer, and M. Giorgetta (2014b), The quasi-biennial oscillation in a warmer climate: Sensitivity to different gravity wave parameterizations, *Clim. Dyn.*, 1–12, doi:10.1007/s00382-014-2314-2.

Soden, B. (2000), The sensitivity of the tropical hydrological cycle to ENSO, *J. Clim.*, *13*, 538–549.

Stevens, B., et al. (2013), Atmospheric component of the MPIM Earth System Model: ECHAM6, *J. Adv. Model. Earth Syst.*, *5*, 1–27, doi:10.1002/jame.20015.

Taguchi, M. (2010), Observed connection of the stratospheric quasi-biennial oscillation with El Niño-Southern Oscillation in radiosonde data, *J. Geophys. Res.*, *115*, D18120, doi:10.1029/2010JD014325.

Taylor, K. E., R. J. Stouffer, and G. A. Meehl (2012), An overview of CMIP5 and the experiment design, *Bull. Am. Meteorol. Soc.*, *93*(4), 485–498, doi:10.1175/BAMS-D-11-00094.1.

Tsuda, T., M. V. Ratnam, S. P. Alexander, T. Kozu, and Y. Takayabu (2009), Temporal and spatial distributions of atmospheric wave energy in the equatorial stratosphere revealed by GPS radio occultation temperature data obtained with the CHAMP satellite during 2001–2006, *Earth Planets Space*, *61*, 525–533.

Wallace, J., R. Panetta, and J. Estberg (1993), Representation of the equatorial stratospheric quasi-biennial oscillation in EOF phase space, *J. Atmos. Sci.*, *50*(12), 1751–1762.

Wang, L., and M. J. Alexander (2010), Global estimates of gravity wave parameters from GPS radio occultation temperature data, *J. Geophys. Res.*, *115*, D21122, doi:10.1029/2010JD013860.

Wang, L., and M. A. Geller (2003), Morphology of gravity-wave energy as observed from 4 years (1998–2001) of high vertical resolution U.S. radiosonde data, *J. Geophys. Res.*, *108*(D16), 4489, doi:10.1029/2002JD002786.

Yuan, W., M. A. Geller, and P. T. Love (2013), ENSO influence on QBO modulations of the tropical tropopause, *Q. J. R. Meteorol. Soc.*, *140*, 1670–1676, doi:10.1002/qj.2247.